J Therm Anal Calorim (2018) 131:873–885
https://doi.org/10.1007/s10973-017-6576-x

Influence of high-volume electric furnace nickel slag and phosphorous slag on the properties of massive concrete

Qiang Wang[1] · Zongxian Huang[1] · Dengquan Wang[1]

Received: 23 May 2017 / Accepted: 12 July 2017 / Published online: 20 July 2017

Abstract This study applied high-volume electric furnace nickel slag (FS), phosphorous slag (PS) and a mixture of the two (FP) to massive concrete, and using fly ash (FA) as the control admixture, investigated the effects of FS and PS on the hydration and hardening process of the cementitious materials, the mechanical properties and the durability of the concrete. Two curing conditions were set, namely the standard curing condition and temperature-matched curing condition (or constant 25 and 50 °C). The hydration heat, hydration products, pore size distribution, mechanical properties and ability of the concrete to resist chloride ion penetration were tested. The results show that the activity of PS and FP is higher than that of FA, while that of FS is lower than that of FA; the improvement of FP on the pore structure of the hardened paste is close to that of FA at late ages under the standard curing condition but better than that of FA at all ages under the temperature-matched curing condition; high-volume FP concrete shows similar or even superior mechanical properties and permeability to chloride ions of concrete to high-volume FA concrete at late ages under both curing conditions.

Keywords Massive concrete · Temperature matching curing · Electric furnace nickel slag · Phosphorous slag

✉ Qiang Wang
w-qiang@tsinghua.edu.cn

[1] Department of Civil Engineering, Tsinghua University, Beijing 100084, China

Introduction

Massive concrete (the dimension at least 120 cm according to ACI 301 [1]) has been widely used in modern construction such as gravity dams, foundation slabs in super high-rise buildings and reactor containment buildings. The hydration heat generated in the central areas of fresh massive concrete is hard to dissipate due to its large volume and poor thermal conductivity, while the heat generated at the concrete surface can dissipate into the surrounding air easily. The temperature gradient from the center to the surface will cause the concrete structures to crack when subjected to restraints [2–4].

Fly ash (FA), a by-product of coal-fired power plants, is mainly composed of Al_2O_3, SiO_2 and Fe_2O_3, and its pozzolanic reaction is quite slow at early ages. To reduce the hydration heat and avoid the cracking of massive concrete, a large part of cement is commonly replaced by fly ash due to its much lower hydration heat [5–9]. Many engineering practices have confirmed that replacing a large part of cement by fly ash is an efficient method to control the temperature rise of massive concrete structures. Wang et al. [10] designed a high-volume fly ash concrete for the foundation slab of a 597-m building in China, and the results showed that the addition of a high amount (45%) of fly ash decreased the temperature rise of concrete significantly and there was no visible cracking on the upper surface of the concrete. In the USA, it has been suggested that fly ash be adopted for the mixture of massive concrete [11]. In Canada, it is recommended to use at least 50% fly ash Type F or CI, or a mixture of both, in massive concrete in hot weather (27 °C) [12].

However, the distribution of industrial residues has remarkable regional characteristics, and the amount of fly ash is quite small in some areas. Therefore, it is necessary

to adopt some other industrial residues in massive concrete to avoid thermal cracking.

Electric furnace ferronickel slag (FS), a by-product of nickel production from nickel oxide ores, consists mainly of SiO_2, MgO, FeO, CaO and Al_2O_3. It is estimated that the annual ferronickel slag output in China is more than 0.8 million tons [13]. However, most of it is disposed of directly in the open environment or treated simply by landfill, which is often considered to be hazardous to ground and underground water. Ioannis et al. [14] summarized that ferronickel slag can be applied in the construction of roads (replacing the limestone aggregates), the production of cement and concrete and other construction materials (e.g., fire-resistant bricks and anti-slip pavement tiles). Among these uses, the use of FS as a raw material for cement production and mineral admixture for concrete should be given priority. However, it was reported that only less than 8% of FS is valuably reused in cement and concrete [13]. The key factor restricting the efficient utilization of FS in cement and concrete is its relatively low activity due to the high SiO_2, MgO, FeO content and low CaO, Al_2O_3 content in its composition.

Phosphorous slag (PS) is generated from yellow phosphor production by the electric furnace method. It is estimated that producing 1 ton of phosphor will generate 7 tons of PS [15], and the annual output of PS is more than 8 million tons in China [16]. PS is mainly composed of CaO, SiO_2, and a small amount of Al_2O_3, P_2O_5 and F. Therefore, it could be used as a suitable raw material for cement production and mineral admixture for concrete. Singh and Bhattacharjee [15] manufactured PS blended cement. It showed comparable strengths and was expected to show low hydration heat. Gao et al. [17] investigated the microstructure of concrete containing superfine PS and found that PS had little cementing action in 7 d, but showed remarkable cementitious properties in 28 d. Chen et al. [18] studied the hydration kinetics of PS-cement paste and concluded that PS substituting parts of cement would reduce hydration products and the total amount of cumulative hydration heat. However, insufficient content of $A1_2O_3$ affects the activity of PS at early ages, and the residual phosphorus in PS can retard the setting time of Portland cement. As a result, PS has not been widely used as the mineral admixture at a high replacement level [19, 20].

Current studies on the properties of concrete containing electric furnace ferronickel slag or phosphorous slag are scarce. In this study, high-volume FS concrete, high-volume PS concrete and high-volume FS-PS (FP) concrete were prepared to investigate their properties. Meanwhile, high-volume fly ash concrete was taken as a control sample because it has been widely used in massive concrete. Additionally, two curing conditions (standard curing condition and temperature-matched curing condition, respectively) were adopted, because for massive concrete, its properties under both the two curing conditions are of great significance.

Experimental

Raw materials

Portland cement with a grade of 42.5 and complying with the Chinese National Standard (GB175-1999), crushed limestone 5–25 mm in size, natural river sand with a fineness of 2.8 mm, polycarboxylic superplasticizer, and three mineral admixtures (fly ash, FS, PS) were used in this study. The chemical compositions of the raw materials are shown in Table 1. Particle size distributions of the raw materials are shown in Fig. 1. XRD patterns of FS and PS

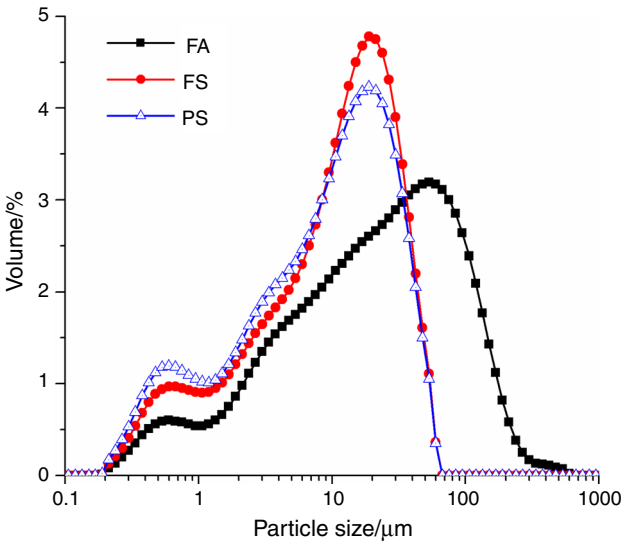

Fig. 1 Particle size distributions of the raw materials

Table 1 Chemical compositions of the raw materials/%

	CaO	SiO_2	Fe_2O_3	Al_2O_3	MgO	MnO	Cr_2O_3	TiO_2	P_2O_5	SO_3	Na_2O	K_2O
Cement	61.20	22.16	4.89	4.18	3.26	0.09	0.04	–	0.03	2.72	0.09	1.23
FA	7.94	47.40	6.43	32.88	0.57	0.14	0.03	1.96	0.11	0.38	0.35	1.16
FS	6.75	46.10	12.25	4.46	27.12	0.79	1.50	0.35	–	0.14	0.15	0.07
PS	40.14	45.39	1.03	3.47	1.97	–	–	0.30	2.61	0.97	1.22	1.70

are shown in Figs. 2 and 3, respectively. There is a hump at about 30° (2θ) in each pattern, which attributed to the presence of amorphous phase. Some crystalline phases (Mg_2SiO_4 for FS and $CaCO_3$, Ca_2SiO_4 and $CaAl_2Si_2O_8$ for PS) can also be identified.

Mix proportions and curing conditions

The water-to-binder (W/B) ratio of the paste and concrete is 0.4. The replacement ratio of cement by mineral admixtures is 50%. Constant 25 and 50 °C were set for the hydration heat test, and standard curing (labeled SC) and temperature-matched curing conditions (labeled TMC) were set for other tests.

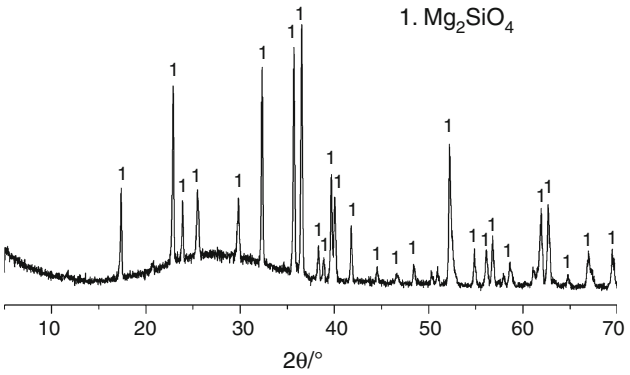

Fig. 2 XRD spectra of the electric furnace ferronickel slag

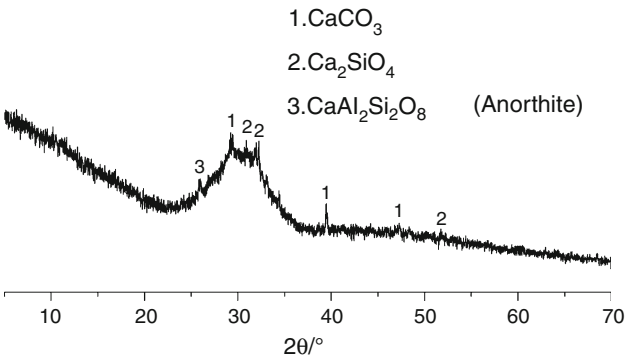

Fig. 3 XRD spectra of the phosphorus slag

The detailed mix proportions of the concrete samples are shown in Table 2.

Test methods

Hydration heat

The rate of hydration heat evolution of the paste was measured using a TAM Air Calorimeter with an accuracy of 20 μw. Two constant temperatures (25 and 50 °C) were adopted.

The adiabatic temperature rise test of the concrete was performed on a 6×10^4 cm^3 specimen with an electric thermometer embedded in its center. The tester maintains the adiabatic condition by circulating air, and it records temperature rise resulting from the concrete hydration every 10 min with an accuracy of 0.1 °C. The results of the adiabatic temperature rise test will be used to provide the basis for temperature-matched curing.

Hydration products

The hydration products of plain cement, FA-cement binder, FS-cement binder and PS-cement binder were mineralogically determined by X-ray diffraction (XRD: TTR III diffractometer). Two testing ages (28 and 90 d) and curing conditions (standard curing and temperature-matched curing) were set. Patterns were obtained on finely ground samples using nickel-filtered CuK α_1 radiation (=1.5405 Å), 45 kV of voltage and 200 mA of current.

A thermogravimetric analysis (TG-DTG) was carried out to measure the $Ca(OH)_2$ content of the hydration product with a TA-Q5000 instrument and a heating rate of 10 °C min^{-1} in a nitrogen atmosphere. Two testing ages (28 and 90 d) were adopted.

Pore size distribution

A mercury intrusion porosimeter (MIP) was used to determine the pore size distributions and total porosities of the hardened pastes. This device, with an operating pressure up to 60,000 Lb in^{-2}, can intrude mercury into pores as small as 3.2 nm in diameter. Three testing ages (3, 28 and 90 d) were adopted.

Table 2 Mix proportions of the concretes/kg m^{-3}

Samples	Cement	Fly ash	Ferronickel slag	Phosphorus slag	Fine aggregates	Coarse aggregates	Water
FA	210	210	0	0	780	1034	168
FS	210	0	210	0	780	1034	168
PS	210	0	0	210	780	1034	168
FP	210	0	105	105	780	1034	168

Mechanical properties

The concrete samples (100 × 100 × 100 mm) were prepared and cured under the standard curing condition (room temperature 20 ± 1 °C and 95 ± 5% relative humidity). The compressive strength, splitting tensile strength and elastic modulus of the concretes were measured at 1, 3, 7, 28, 56 and 90 d.

Ability of the concrete samples to resist chloride ion penetration

The permeability of the concrete samples to chloride ions was tested according to International Standard ASTM C1202. The electrical conductance of the concrete samples with dimensions of 100 × 100 × 50 mm was tested by an electron flux determinator at 28 and 90 d.

Results and discussion

Hydration heat

Figure 4 shows the exothermic rates of the FA-cement, FS-cement, PS-cement and FP-cement cementitious materials at 25 and 50 °C. At 25 °C, the main heat evolution peak of FS-cement binder occurs earlier than that of FA-cement binder, indicating that the activity of FS as mineral admixture is higher than that of FA at the initial stage. The appearance of the main heat evolution peaks of PS-cement and FP-cement binders is later than that of FA-cement binder, indicating that PS has a retarding effect on the hydration of cement [21–23]. The main reasons for this retarding effect may include that PO_4^{3-} anion from PS can react with Ca^{2+} cation, and they precipitate as $Ca_{10}(PO_4)_6(OH)_2$, instead of $Ca(OH)_2$ [24]; the reaction of PO_4^{3-} anion and Ca^{2+} cation can form calcium dihydrogen and hydrogen phosphate, resulting in the deficiency of calcium ions in the solution, which causes the nucleation and the growth of the CSH phase to be poisoned [22]; the presence of residual phosphorus results in forming phosphoric acid that can lower the PH value and provide negative effects on the hydration of cement [25]. Additionally, P–O bonds in PS are stronger than Si–O or Al–O bonds and more difficult to break, resulting in the relatively low early-age activity of PS [26]. Some other studies revealed that high-volume fly ash also has a retarding effect on the hydration of cement at early ages due to the dilution effect and relatively low activity of fly ash [27–30]. In comparison, PS presents a much more obvious retarding effect on the hydration of cement.

At 50 °C, the main heat evolution peaks of FA-cement, FS-cement, PS-cement and FP-cement binders appear much earlier than that at 25 °C. In addition, the peak values of binders at 50 °C are much higher. This indicates that improving temperature can significantly promote the hydration of the binders. The occurrence order of the main heat evolution peaks of the four binders at 50 °C is the same as that at 25 °C, but the time between the two adjacent peaks is shortened (from 2.69–4.96 h at 25 °C to 1.16–1.84 h at 50 °C) because of the activated effects of high temperature.

Figure 5 shows the 7 d cumulative hydration heats of FA-cement, FS-cement, PS-cement and FP-cement binders

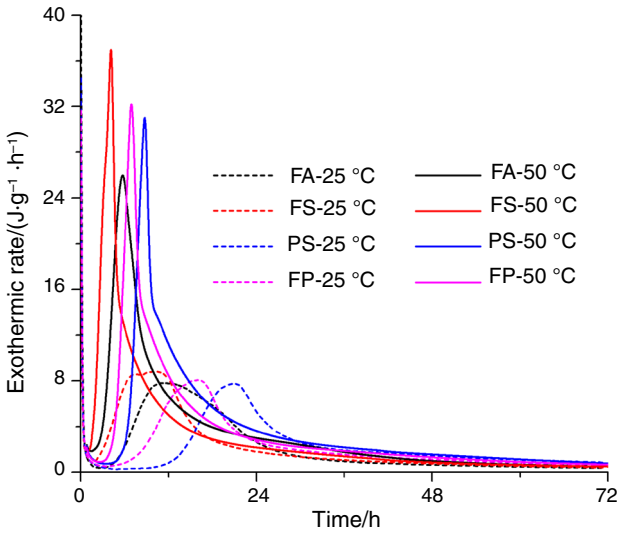

Fig. 4 Heat evolution of the FA-cement, FS-cement, PS-cement and FP-cement cementitious materials under constant temperatures (25 and 50 °C)

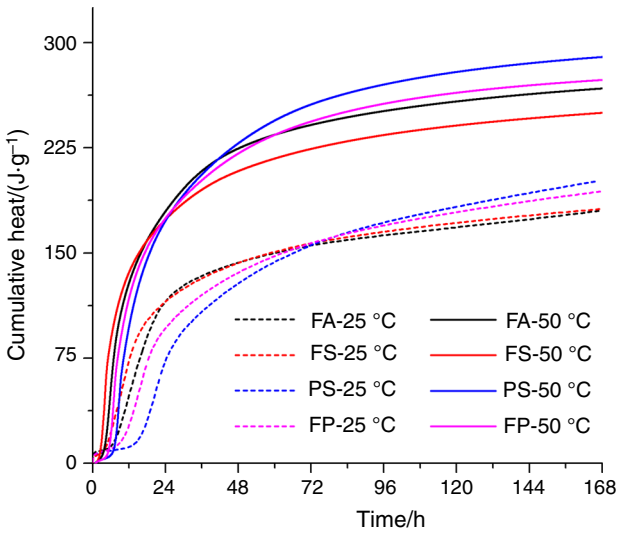

Fig. 5 Cumulative hydration heat of the FA-cement, FS-cement, PS-cement and FP-cement cementitious materials under constant temperatures (25 and 50 °C)

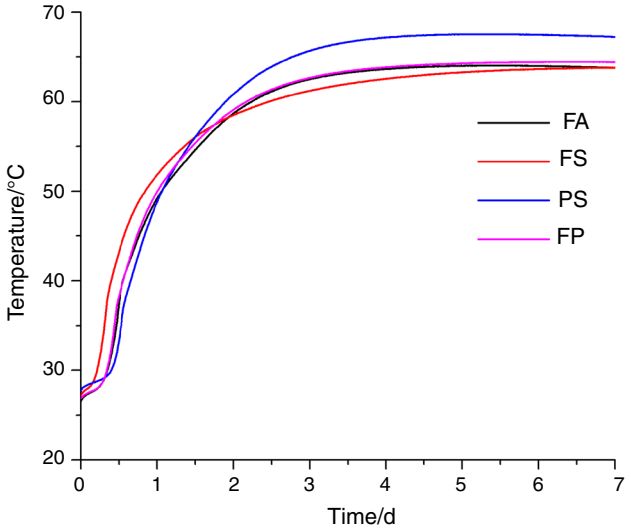

Fig. 6 Adiabatic temperature rises of the FA-cement, FS-cement, PS-cement and FP-cement concrete samples

at 25 and 50 °C. The cumulative hydration heat of FS-cement binder is close to at 25 °C, but significantly lower than at 50 °C that of FA-cement binder, indicating that the activated effect of elevated curing temperature on the early-age activity of fly ash is greater than that of electric furnace ferronickel slag. At both 25 and 50 °C, the cumulative hydration heats of PS-cement and FP-cement binders are lower than that of FA-cement binder at initial stages, but then it is higher. Moreover, the time point at which the cumulative hydration heat of the binders containing PS surpasses that of FA-cement binder occurs earlier.

Figure 6 shows the adiabatic temperature rises of the FA-cement, FS-cement, PS-cement and FP-cement concretes. The hydration temperature of cementitious materials keeps rising due to adiabatic environment. Thus, the rules of the adiabatic temperature rise of concretes are more similar to those of cumulative hydration heat of binders at higher temperature (namely 50 °C). The 7 d adiabatic temperature rises of FA-cement, FS-cement, PS-cement and FP-cement concretes are 37.2, 36.6, 39.6 and 37.5 °C, respectively, which is coincident with the order of 7 d cumulative hydration heat of corresponding cementitious materials at 50 °C. At initial stages, the temperature rise of FA-cement concrete is slower than that of FS-cement concrete while faster than that of PS-cement concrete, which is consistent with the results of the hydration heat of corresponding cementitious materials. The temperature development of FP-cement concrete is similar to that of FA-cement concrete, and the 7 d adiabatic temperature rise is very close to that of FA-cement.

Hydration products

XRD results of the hydration products of FA-cement, FS-cement, PS-cement and FP-cement binders under standard and temperature-matched curing conditions at 90 d are given in Fig. 7. Under the standard curing condition, similar crystalline hydration products, viz. $Ca(OH)_2$, AFt and AFm, are observed in Fig. 7a–d, and there is no new crystalline phase in the hydration products of the hardened pastes. Additionally, the phases of unreacted cement particles and mineral admixtures can be observed, including $3Al_2O_3{\cdot}2SiO_2$ in fly ash and Mg_2SiO_4 in electric furnace ferronickel slag. Under the temperature-matched curing condition, the crystalline phases in the hardened pastes are similar to that under the standard curing condition, but the intensity of the $Ca(OH)_2$ characteristic peak of the binders is much lower than that under the standard curing condition. This is mainly because fly ash, electric furnace ferronickel slag and phosphorous slag can consume the $Ca(OH)_2$ in the cementitious system due to their pozzolanic activities, which can be significantly enhanced by elevated temperature.

Figures 8 and 9 show the TG and DTG curves of the binders at 28 and 90 d, respectively. (a) and (b) represent standard and temperature-matched curing conditions, respectively. It can be seen from the TG and DTG curves that there is an obvious endothermic peak for all the samples at approximately 400–500 °C corresponding to the dehydration of $Ca(OH)_2$.

Figure 10 shows the $Ca(OH)_2$ content calculated according to the TG and DTG results. At 28 d, the $Ca(OH)_2$ contents of the FS-cement, PS-cement and FP-cement hardened pastes are all higher than that of the FA-cement hardened paste under the standard curing condition, indicating that electric furnace ferronickel slag and phosphorous slag consume less $Ca(OH)_2$ than fly ash. Under the temperature-matched curing condition, fly ash still consumes the largest amount of $Ca(OH)_2$. The $Ca(OH)_2$ contents of the FA-cement, FS-cement, PS-cement and FP-cement hardened pastes under temperature-matched curing are 21.74, 12.36, 3.98 and 4.30% lower than that under the standard curing condition, respectively. This indicates that high temperature can promote the pozzolanic reaction of fly ash, electric furnace ferronickel slag and phosphorous slag, which is consistent with the XRD results. It also indicates that this promotion is much more significant on fly ash. At 90 d, the results of $Ca(OH)_2$ contents of the four hardened pastes are similar to those at 28 d. The $Ca(OH)_2$ contents of the FS-cement, PS-cement and FP-cement hardened pastes are all higher than that of the FA-cement hardened paste under both standard and temperature-matched curing conditions. The $Ca(OH)_2$ contents of the FA-cement, FS-cement, PS-cement and FP-cement hardened

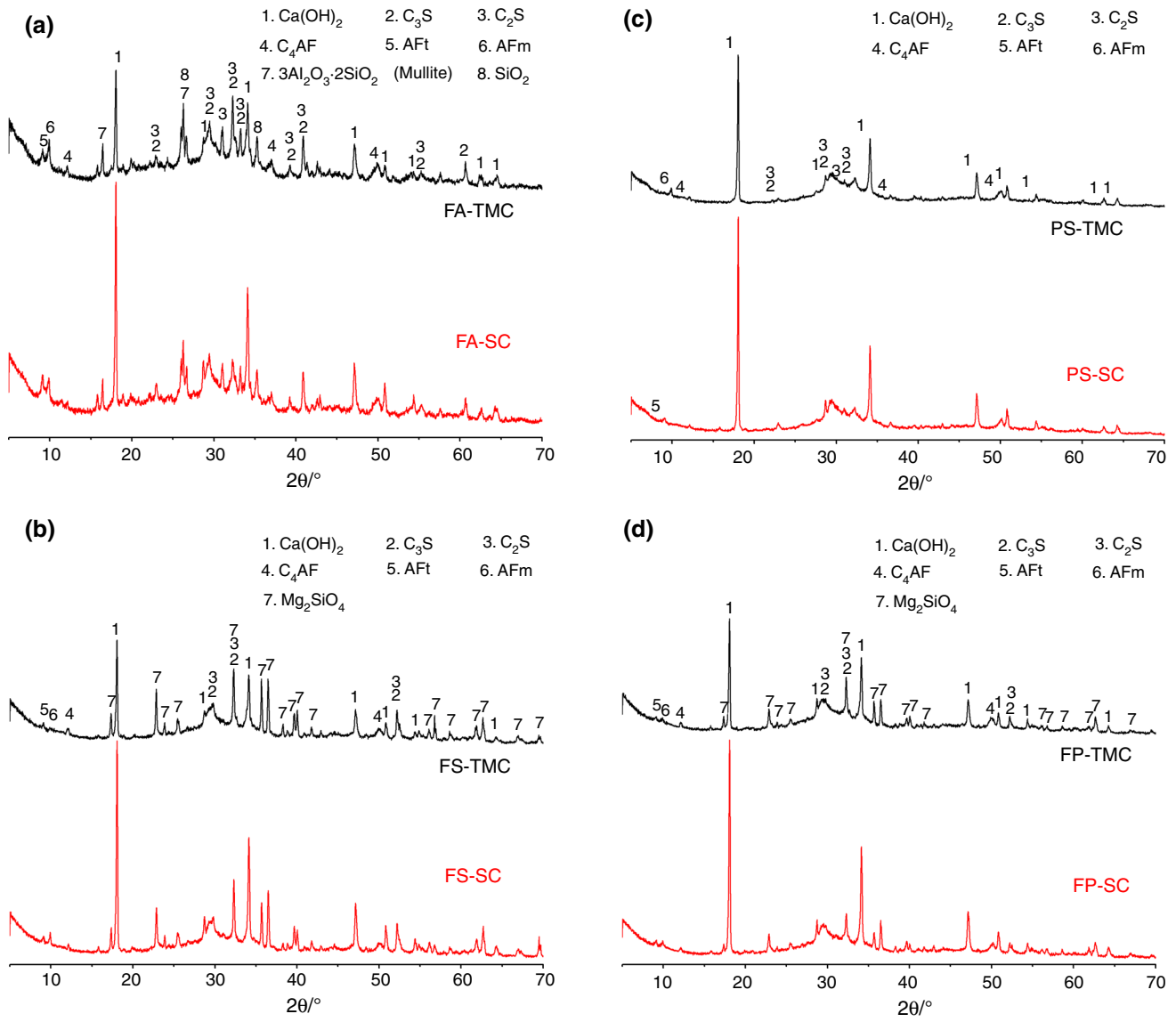

Fig. 7 XRD patterns of the binders under standard and temperature-matched curing conditions at 90 d. **a** FA-cement binder, **b** FS-cement binder, **c** PS-cement binder and **d** FP-cement binder

pastes under temperature-matched curing are 22.07, 9.11, 3.45 and 6.49% lower than that under the standard curing condition, respectively. Furthermore, the $Ca(OH)_2$ content of the FA-cement hardened paste at 90 d is lower than that at 28 d, while the contents of the FS-cement, PS-cement and FP-cement hardened pastes are almost unchanged from 28 to 90 d. This indicates that the amount of $Ca(OH)_2$ produced by cement hydration is less than that consumed by fly ash but more than that consumed by electric furnace ferronickel slag and phosphorous slag.

Pore structure

Figures 11–13 show the cumulative pore volumes of the hardened pastes at 3, 28 and 90 d. (a) and (b) represent the standard and temperature-matched curing conditions, respectively. At 3 d, under the standard curing condition, the cumulative pore volumes of the FS-cement and FP-cement hardened pastes are both larger than that of the FA-cement hardened paste, while the cumulative pore volume and the most probable aperture of the PS-cement hardened paste are slightly smaller than those of the FA-cement hardened paste. This indicates that phosphorous slag is of high activity and can produce more hydration products to fill pores at 3 d. Under the temperature-matched curing condition, the cumulative pore volume and the most probable aperture of the FS-cement hardened paste are significantly larger than those of the FA-cement hardened paste, while those of the PS-cement hardened paste are obviously smaller than those of the FA-cement hardened

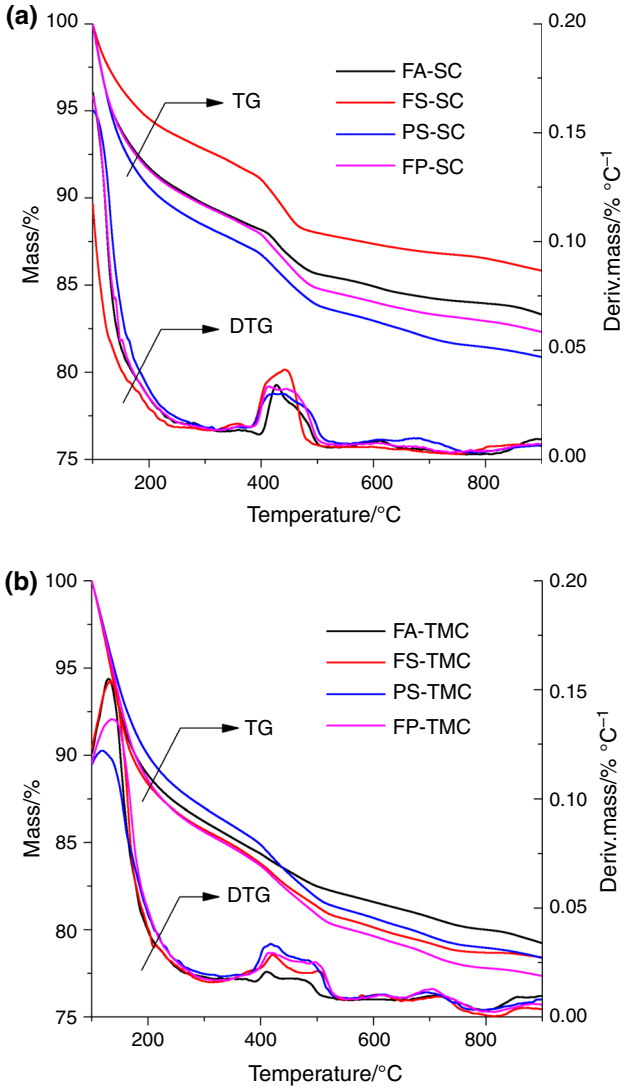

Fig. 8 TG and DTG curves of the FA-cement, FS-cement, PS-cement and FP-cement binders at 28 d. Under the **a** standard curing condition and **b** temperature-matched curing condition

paste. The cumulative pore volume and the most probable aperture of the FP-cement hardened paste are slightly smaller than those of the FA-cement hardened paste, which is different from the results under the standard curing condition. This indicates that high temperature can significantly promote the hydration of the FP-cement binder (especially phosphorous slag in the binder).

At 28 d, under the standard curing condition, the cumulative pore volume and the most probable aperture of the FS-cement hardened paste are larger than those of the FA-cement hardened paste, while those of the PS-cement hardened paste are smaller than those of the FA-cement hardened paste. The most probable aperture and harmful pore (>50 nm) volume of the FP-cement hardened paste are close to those of the FA-cement hardened paste, though its cumulative pore volume is larger than that of the FA-cement hardened paste. This indicates that with increasing age, the FP-cement binder produces more hydration products to fill pores. Under the temperature-matched curing condition, the results are similar to those at 3 d, but the cumulative pore volumes of the four hardened pastes are reduced by approximately 0.05 mL g^{-1} compared with those at 3 d.

At 90 d, under the standard curing condition, cumulative pore volumes of the FS-cement and FP-cement hardened pastes are larger than those of the FA-cement hardened paste, while those of the PS-cement hardened paste are smaller than those of the FA-cement hardened paste, which is similar to the results at 28 d. However, cumulative harmful pore (>50 nm) volumes of the FS-cement, PS-cement and FS-cement hardened pastes are the same as that of the FA-cement hardened paste. Under the temperature-matched curing condition, the cumulative pore volume and the most probable aperture of the FS-cement hardened paste are larger than those of the FA-cement hardened paste, but the cumulative harmful pore (>50 nm) volume is the same as that of the FA-cement hardened paste. The cumulative pore and harmful pore (>50 nm) volumes and the most probable aperture of the PS-cement and FP-cement hardened pastes are significantly smaller than those of the FA-cement hardened paste. This indicates that at 90 d, the pore structures of the PS-cement and FP-cement hardened pastes are better than that of the FA-cement hardened paste under the temperature-matched curing condition.

Above all, the contribution of electric furnace ferronickel slag to the pore structure of the hardened paste is less than that of fly ash at both standard and temperature-matched curing conditions, but the gap between the two decreases with the increase in age. The contribution of phosphorous slag to the pore structure is more than that of fly ash, and it is much more significant under the temperature-matched curing conditions. Under the standard curing condition, ferronickel slag–phosphorous slag composite cementitious material makes less contribution to the early-age pore structure than fly ash, but its contribution is close to that of fly ash at the late age; under the temperature-matched curing condition, the contribution of ferronickel slag–phosphorous slag composite cementitious material is close to that of fly ash at early ages but is significantly greater at the late age.

Mechanical properties

Figure 14 shows the compressive strengths of the FA-cement, FS-cement, PS-cement and FP-cement concrete samples under standard and temperature-matched curing conditions. Under the standard curing condition, the compressive strength of the PS-cement concrete is obviously lower than that of the FA-cement concrete at 1 d due to the

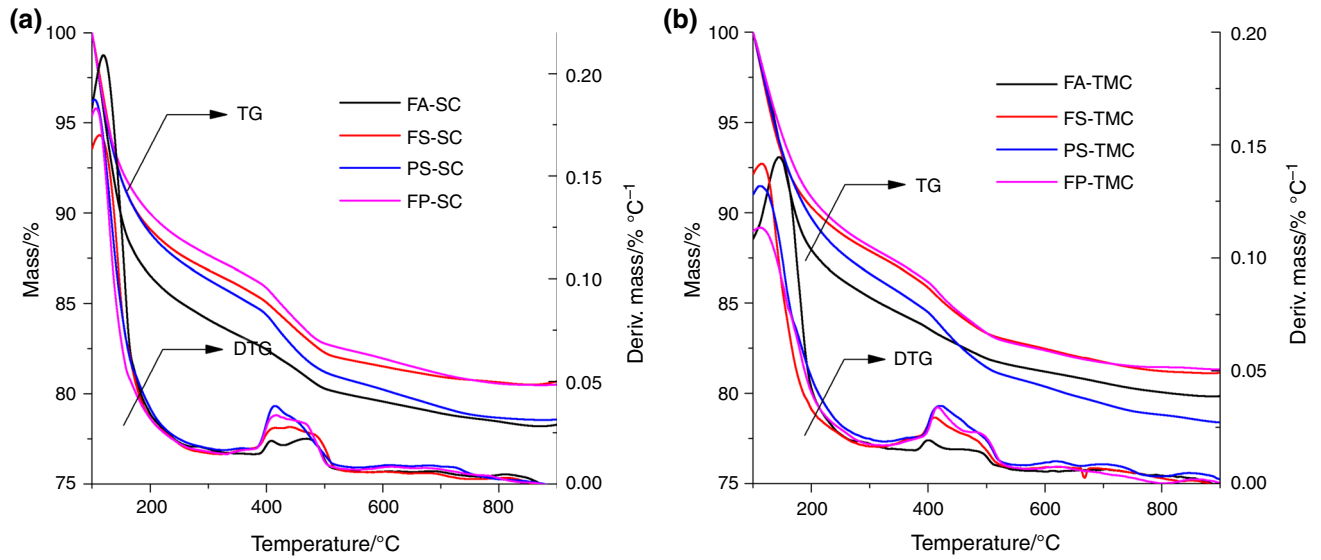

Fig. 9 TG and DTG curves of the FA-cement, FS-cement, PS-cement and FP-cement binders at 90 d. Under the **a** standard curing condition and **b** temperature-matched curing condition

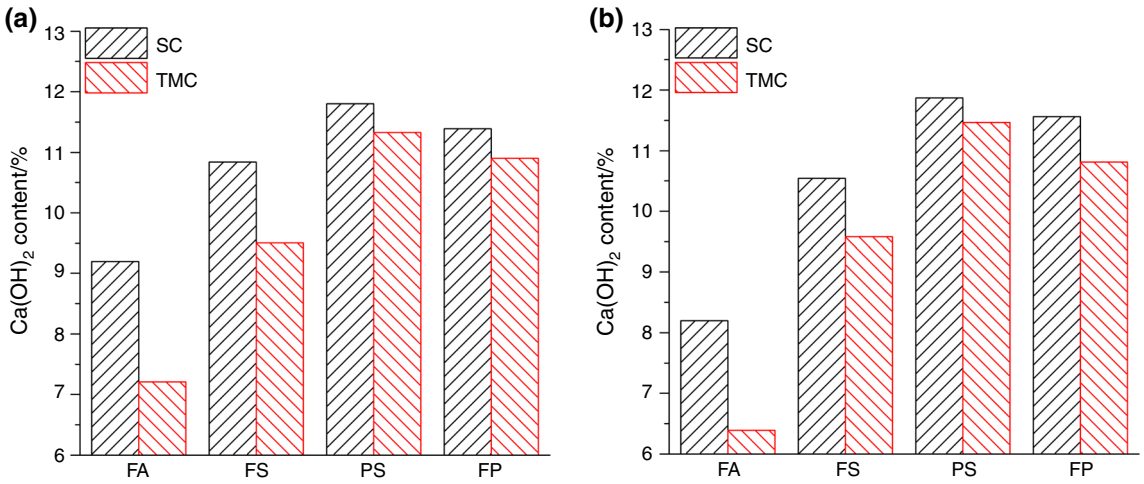

Fig. 10 $Ca(OH)_2$ content of the FA-cement, FS-cement, PS-cement and FP-cement binders under standard and temperature-matched curing conditions at **a** 28 d and **b** 90 d

retarding effect of phosphorous slag, but it is close to that of FA-cement concrete at 3 d. After 7 d, the compressive strength of PS-cement concrete is significantly higher than that of FA-cement concrete, indicating that phosphorous slag is of higher activity. This result is consistent with the hydration heat result of the PS-cement cementitious material and the pore structure result of the PS-cement hardened paste. The compressive strength of the FS-cement concrete is close to that of the FA-cement concrete within 7 d but obviously lower after 7 d under the standard curing condition, indicating that electric furnace ferronickel slag is of relatively lower activity. This result is also consistent with the hydration heat result of FS-cement cementitious material and the pore structure result of the FS-cement hardened paste. The compressive strength of the FP-cement concrete is close to that of the FA-cement concrete within 3 d but higher after 3 d under the standard curing condition. Under the temperature-matched curing condition, the compressive strength growth at early ages increases, and the 3 d compressive strength can reach 61.39–69.62% of the 90 d compressive strength, while the proportion under the standard curing condition is 33.94–38.39%. This result indicates that high temperature can significantly promote the hydration of cement and the four mineral admixtures, which is consistent with the results of hydration heat, XRD and pore structure. The compressive strength of the PS-cement concrete is lower at 1 d but significantly higher after 3 d than that of the FA-cement concrete under

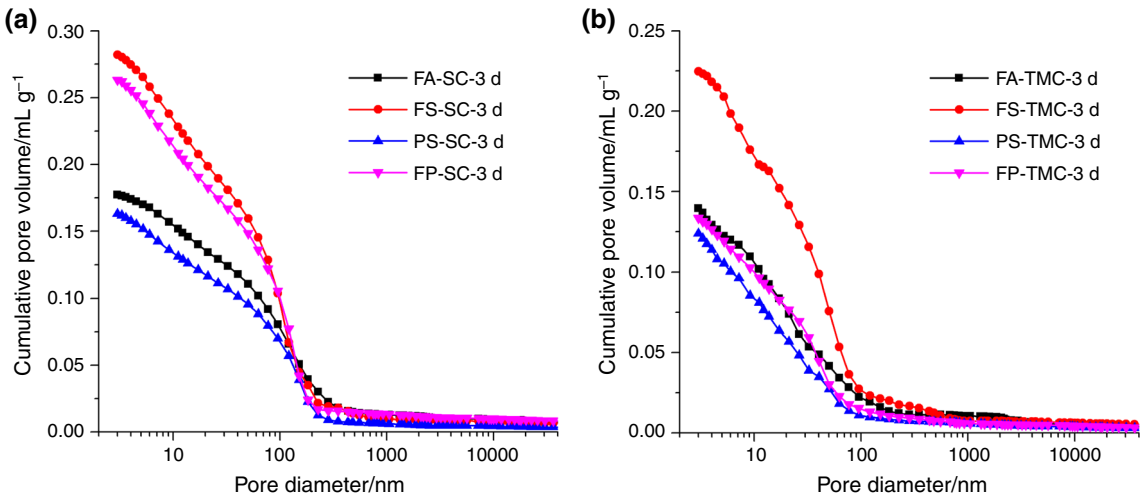

Fig. 11 Cumulative pore volume of the FA-cement, FS-cement, PS-cement and FP-cement hardened pastes at 3 d under the **a** standard curing condition and **b** temperature-matched curing condition

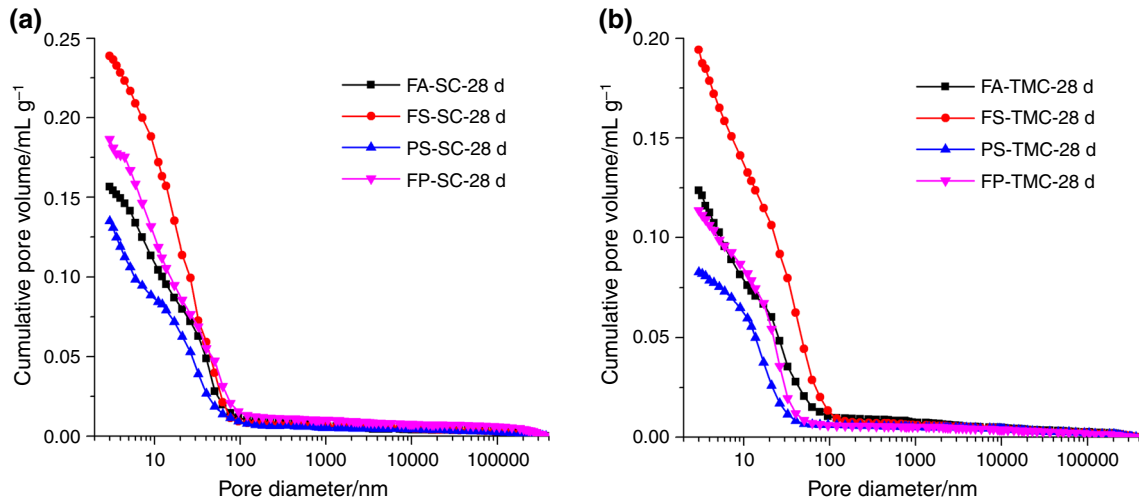

Fig. 12 Cumulative pore volume of the FA-cement, FS-cement, PS-cement and FP-cement hardened pastes at 28 d under the **a** standard curing condition and **b** temperature-matched curing condition

temperature-matched curing conditions. The compressive strength of the FS-cement concrete is higher at 1 d but obviously lower after 3 d than that of FA-cement concrete. Furthermore, the compressive strength of FP-cement concrete is close to that of FA-cement concrete within 56 d but slightly higher than that of FA-cement concrete at 90 d.

Figure 15 shows the splitting tensile strengths of the FA-cement, FS-cement, PS-cement and FP-cement concretes under the standard and temperature-matched curing conditions. The result is similar to that of compressive strength. Under the standard curing condition, the splitting tensile strength of the PS-cement concrete is obviously lower than that of the FA-cement concrete at 1 d but higher after 7 d; the splitting tensile strength of the FS-cement concrete is close to that of the FA-cement concrete within 7 d but obviously lower than that of the FA-cement concrete after 7 d; the strength development of the FP-cement concrete is close to that of the FA-cement concrete. Under the temperature-matched curing condition, the rule is similar to that under the standard curing condition, but the FP-cement concrete presents higher 90 d splitting tensile strength than the FA-cement concrete. Moreover, the increase in splitting tensile strength increases at early ages, and the 3 d splitting tensile strength can reach 65.70–75.40% of the 90 d compressive strength, while the proportion under the standard curing condition is 44.13–50.38%.

Figure 16 shows the elastic modulus of the FA-cement, FS-cement, PS-cement and FP-cement concretes under the standard and temperature-matched curing conditions.

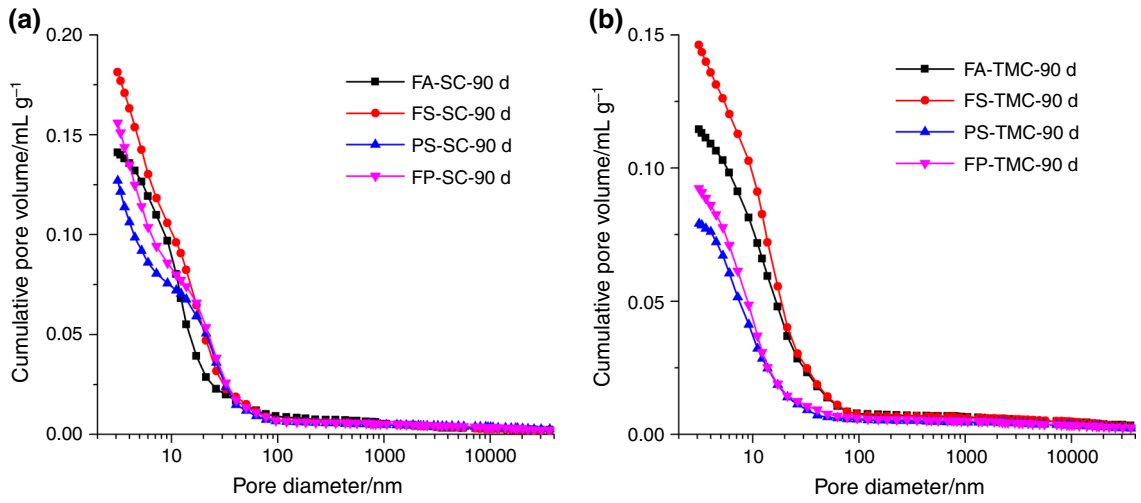

Fig. 13 Cumulative pore volume of the FA-cement, FS-cement, PS-cement and FP-cement hardened pastes at 90 d under the **a** standard curing condition and **b** temperature-matched curing condition

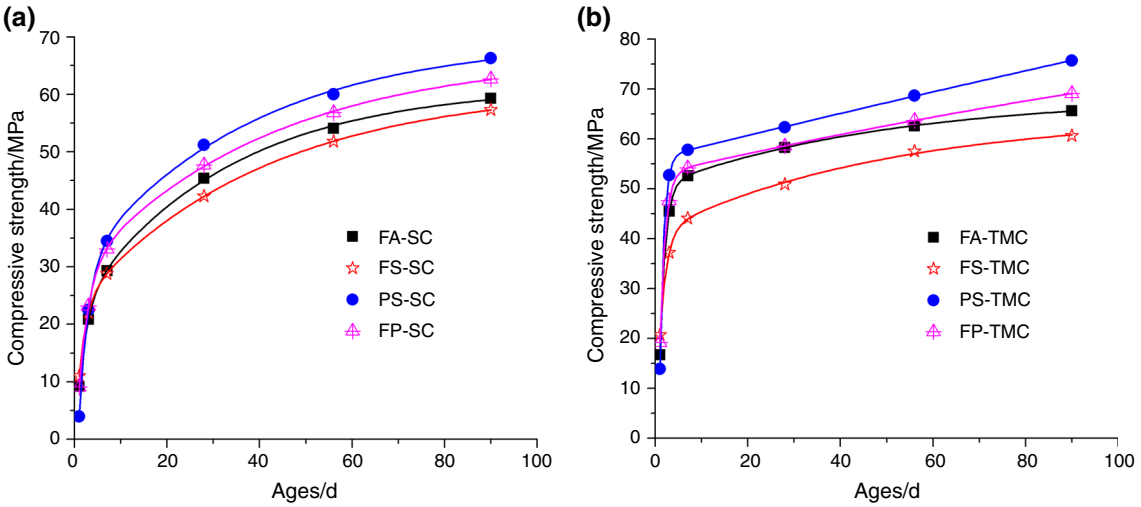

Fig. 14 Compressive strength of concrete samples under the **a** standard curing condition and **b** temperature-matched curing condition

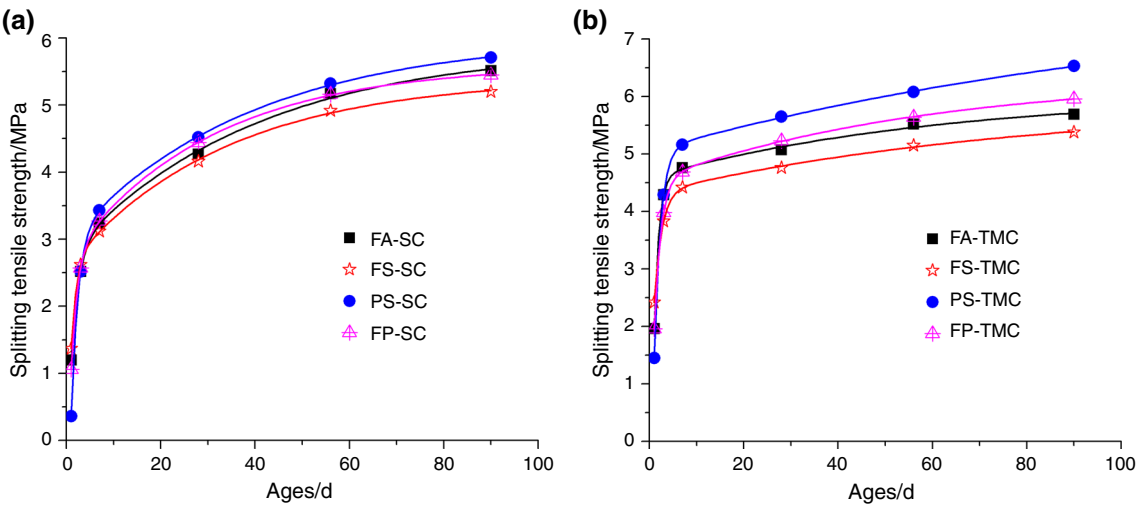

Fig. 15 Splitting tensile strength of concrete samples under the **a** standard curing condition and **b** temperature-matched curing condition

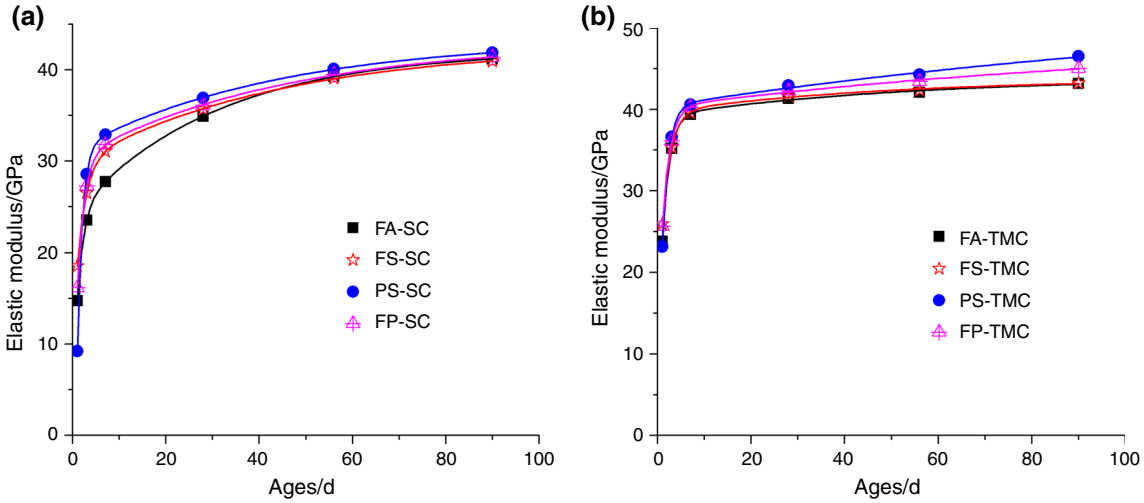

Fig. 16 Elastic modulus of concrete samples under the **a** standard curing condition and **b** temperature-matched curing condition

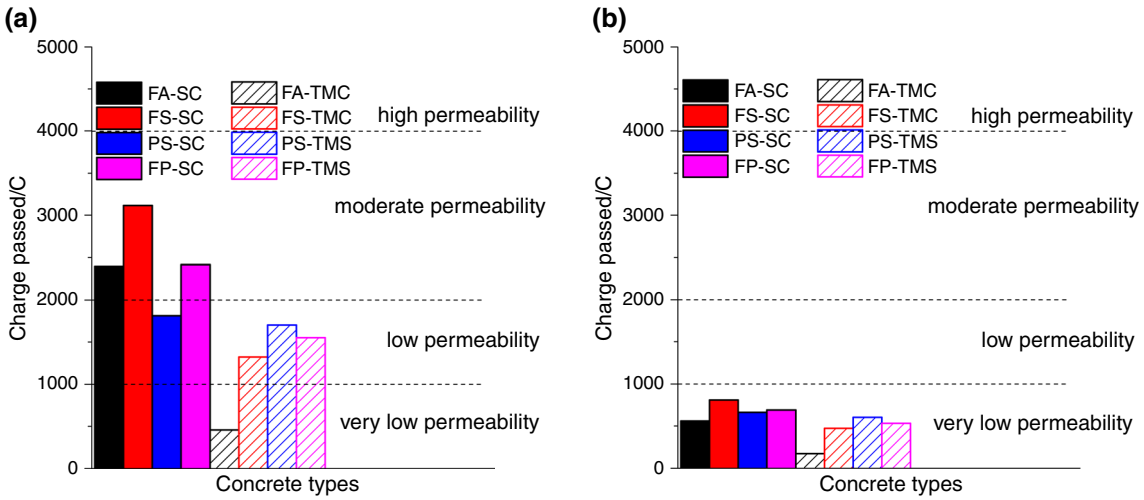

Fig. 17 Chloride ion permeability of concrete samples under standard and temperature-matched curing conditions at **a** 28 d and **b** 90 d

Under the standard curing condition, the elastic modulus of the FS-cement, PS-cement and FP-cement concretes is close to that of the FA-cement concrete after 56 d, but the development of the elastic modulus is different for different concretes at early ages. The PS-cement concrete presents an obviously lower elastic modulus than that of the FA-cement concrete at 1 d due to the retarding effect of phosphorous slag, but its elastic modulus is higher than that of the FA-cement concrete after 3 d; the elastic modulus of the FS-cement and FP-cement concrete samples is always higher than that of the FA-cement concrete before 28 d. Under the temperature-matched curing condition, the FS-cement, PS-cement and FP-cement concretes present similar elastic modulus with the FA-cement concrete before 7 d, which is different from the result under the standard curing condition. This is because high temperature can significantly promote the reaction of cementitious materials. After 7 d, the elastic modulus of the PS-cement and FP-cement concretes is 7.78 and 4.31% higher than that of the FA-cement concrete, respectively, while that of the FS-cement is always close to that of the FA-cement concrete.

Above all, the mechanical properties of concrete containing a high volume of phosphorous slag are similar or even superior to those of the FA-cement concrete, while those of the FS-cement concrete are not as good as those of FA-cement concrete.

Ability of concrete to resist chloride ion penetration

Figure 17a and b shows the chloride ion permeability of concretes at 28 and 90 d, respectively. At 28 d, under the standard curing condition, the chloride ion permeability of

the PS-cement concrete ("low") is one level lower than that of the FA-cement, FS-cement and FP-cement concretes ("moderate"). This result indicates that phosphorous slag is of relatively higher activity, which is consistent with the results of hydration heat and pore structure. Under the temperature-matched curing condition, the level of chloride ion permeability of the FA-cement concrete is reduced to "very low" and those of the FS-cement and FP-cement concretes are reduced to "low," while that of PS-cement concrete remains "low." This indicates that temperature-matched curing can greatly improve the resistance to chloride ion permeability of the FA-cement, FS-cement and FP-cement concretes. Among them, the improvements in the FA-cement and PS-cement concretes are the most and least obvious, respectively. At 90 d, the level of chloride ion permeability of the four types of concretes is "very low" under both the standard and temperature-matched curing conditions.

Conclusions

1. Based on the results of hydration heat, it can be concluded that the activity of phosphorous slag is higher than that of fly ash, while that of ferronickel slag lower than that of fly ash. Furthermore, the activity of ferronickel slag–phosphorous slag composite material (1:1 by mass) is higher than that of fly ash under both standard and temperature-matched curing conditions. Additionally, the adiabatic temperature rise of concrete containing high-volume ferronickel slag–phosphorous slag composite material (FP-cement concrete) is close to that of concrete containing high-volume fly ash.
2. The thermal analysis shows that fly ash can consume more $Ca(OH)_2$ than ferronickel slag, phosphorous slag and ferronickel slag–phosphorous slag composite material. Besides, the four mineral admixtures can consume more $Ca(OH)_2$ under temperature-matched curing condition than under standard curing condition.
3. At late ages, ferronickel slag–phosphorous slag composite material makes a greater contribution to pore structure than fly ash under temperature-matched curing condition, and similar contribution with fly ash under standard curing condition; however, the contribution of the composite material is not as good as that of fly ash at early ages, especially under the standard curing condition.
4. The mechanical properties of the FP-cement concrete are similar or even superior to those of the FA-cement concrete based on the results of compressive strength, splitting tensile strength, elastic modulus and the chloride ion permeability of concretes.
5. Ferronickel slag–phosphorous slag composite material presents similar or even superior properties to fly ash when used in massive concrete, and it is a potential high-quality mineral admixture for massive concrete.

Acknowledgements This work was supported by the Tsinghua University Initiative Scientific Research Program [Grant Number 20161080079] and the Jiangsu Key Laboratory of Construction Materials [Grant Number CM2016-02].

Compliance with ethical standards

Conflict of interest The authors declare that they have no conflict of interest.

References

1. ACI Committee 301–10. Specification for structure concrete. Farmington Hills, MI: American Concrete Institute; 2010.
2. Chu I, Lee Y, Amin MN, Jang B, Kim J. Application of a thermal stress device for the prediction of stresses due to hydration heat in mass concrete structure. Constr Build Mater. 2013;45:192–8.
3. Li Y, Nie L, Wang B. A numerical simulation of the temperature cracking propagation process when pouring mass concrete. Automat Constr. 2014;37:203–10.
4. Zhang G, Li G. Effects of mineral admixtures and additional gypsum on the expansion performance of sulphoaluminate expansive agent at simulation of mass concrete environment. Constr Build Mater. 2016;113:970–8.
5. Du C. Dam construction–concrete temperature control using fly ash. Concr Int. 1996;18:34–6.
6. Langan BW, Weng K, Ward MA. Effect of silica fume and fly ash on heat of hydration of Portland cement. Cement Concr Res. 2002;32(7):1045–51.
7. Mengxiao S, Qiang W, Zhikai Z. Comparison of the properties between high-volume fly ash concrete and high-volume steel slag concrete under temperature matching curing condition. Constr Build Mater. 2015;98:649–55.
8. Liu SH, Wang L, Gao YX, Yu BY, Bai Y. Comparing study on hydration properties of various cementitious systems. J Therm Anal Calorim. 2014;118(3):1483–92.
9. Zhang TS, Yu QJ, Wei JX. Improvement of surface cementitious properties of coarse fly ash by dehydration and rehydration processes. J Therm Anal Calorim. 2012;109(1):265–71.
10. Wang Q, Yan PY, Feng JJ. Design of high-volume fly ash concrete for a massive foundation slab. Mag Concr Res. 2013;65(2):71–81.
11. Florida DOT. Standard specifications for road and bridge construction. Tallahassee, FL: Florida Department of Transportation; 2017.
12. Bobkracino CP, Seracino R, Zia P, Edwards A. Crack free mass concrete footings on bridges in coastal environments, NCDOT Project 2012–09 (FHWA/NC/2012-09).: Department of Civil, Construction, and Environmental Engineering, North Carolina State University, 2014.
13. Zhang Z, Zhu Y, Yang T, Li L, Zhu H, Wang H. Conversion of local industrial wastes into greener cement through geopolymer technology: a case study of high-magnesium nickel slag. J Clean Prod. 2017;141:463–71.
14. Maragkos I, Giannopoulou IP, Panias D. Synthesis of ferronickel slag-based geopolymers. Miner Eng. 2009;22(2):196–203.
15. Singh NB, Bhattacharjee KN. Phosphorous furnace slag—a potential waste material for the manufacture of cements. Indian J Eng Mater S. 1996;3:41–4.
16. Zhang XW, Yang L, Zhang B. Utilization of phosphorus slag and fly ash for the preparation of ready-mixed mortar. Appl Mech Mater. 2013;423–426:987–92.

17. Gao PW, Lu XL, Yang CX, Li XY, Shi NN, Jin SC. Microstructure and pore structure of concrete mixed with superfine phosphorous slag and superplasticizer. Constr Build Mater. 2008;22(5):837–40.
18. Chen X, Fang KH, Yang HQ, Peng H. Hydration kinetics of phosphorus slag–cement paste. J Wuhan Univ Technol. 2011; 26(1):142–6.
19. Li DX, Shen JL, Mao LX, Wu XQ. The influence of admixtures on the properties of phosphorous slag cement. Cement Concr Res. 2000;30(7):1169–73.
20. Allahverd A, Pilehva S, Mahinroosta M. Influence of curing conditions on the mechanical and physical properties of chemically-activated phosphorous slag cement. Powder Technol. 2016;288:132–9.
21. Li D, Shen J, Mao L, Wu X. The influence of admixtures on the properties of phosphorous slag cement. Cement Concr Res. 2000;30(7):1169–73.
22. Kalina L, Bílek V, Novotný R, Monček ová M, Másilko J, Koplík J. Effect of Na3PO4 on the hydration process of alkali-activated blast furnace slag. Materials. 2016;9(5):395.
23. Dongxu L, Jinlin S, Lin C, Xuequan W. The influence of fast-setting/early-strength agent on high phosphorous slag content cement. Cement Concr Res. 2001;31(1):19–24.
24. Lee WKW, van Deventer JSJ. Effects of anions on the formation of aluminosilicate gel in geopolymers. Ind Eng Chem Res. 2002;41(18):4550–8.
25. Allahverdi A, Pilehvar S, Mahinroosta M. Influence of curing conditions on the mechanical and physical properties of chemically-activated phosphorous slag cement. Powder Technol. 2016;288:132–9.
26. Shi C, Qian J. High performance cementing materials from industrial slags—a review. Resour Conserv Recycl. 2000;29(3): 195–207.
27. Dakhane A, Tweedley S, Kailas S, Marzke R, Neithalath N. Mechanical and microstructural characterization of alkali sulfate activated high volume fly ash binders. Mater Des. 2017;122:236–46.
28. Ng S, Justnes H. Influence of plasticizers on the rheology and early heat of hydration of blended cements with high content of fly ash. Cem Concr Compos. 2016;65:41–54.
29. Thongsanitgarn P, Wongkeo W, Chaipanich A, Poon CS. Heat of hydration of Portland high-calcium fly ash cement incorporating limestone powder: effect of limestone particle size. Constr Build Mater. 2014;66:410–7.
30. Liu SH, Kong YI, Wang L. A comparison of hydration properties of cement—low quality fly ash binder and cement—limestone powder binder. J Therm Anal Calorim. 2014;116(2):937–43.